JOINT INSTITUTE FOR NUCLEAR RESEARCH

Bogoliubov Laboratory of Theoretical Physics (BLTP)

FINAL REPORT ON THE START PROGRAMME

Numerical Simulation of IV - Characteristics in Anomalous Josephson Junction Under Electromagnetic Radiation

Group Supervisor:
Prof. Yu. M .Shukrinov
BLTP, JINR, Dubna, Russia

START Supervisor:
Dr. Majed Nashaat
BLTP, JINR, Dubna, Russia

Student:
Hala Alsayad (Master's student) Cairo University, Department of Physics
Giza, Egypt

Participation period:

2 July - 26 August, 2023

Dubna 2023

Abstract

In this study we investigate the phase and magnetization dynamics of a superconductor-ferromagnet-superconductor (SFS) anomalous Josephson junction with a Rashba type spin-orbit coupling (SOC). We demonstrate some interesting features including the appearance of a negative differential resistance region in the current-voltage characteristics (CVC) curves, corresponding to it a ferromagnetic resonance (FMR) is observed. The application of the electric component of an electromagnetic radiation (EMR) demonstrated a locking phenomena with constant magnetization and the ability to control the magnetization precession. The application of the magnetic component also demonstrated locking but with varying magnetization amplitude. In this study we investigate the effect of both EMR components together. We show the ability to control the width of the locking region for some parameters. Our results are through numerical simulations solving the coupled system of Landau-Lifshitz-Gilbert (LLG) and Josephson equations using a fourth order Runge-Kutta method.

Contents

1 Introduction

The dynamics of a superconductor-insulator-superconductor (SIS) Josephson junction are described through the two Josephson relations, the current-phase relation (CPR) and the voltage phase relation given respectively by

$$\begin{aligned} I_s &= I_c \sin\varphi \\ \frac{\partial\varphi}{\partial t} &= \frac{2\pi}{\Phi_o} V \end{aligned} \tag{1}$$

where I_c is the critical current of the junction, φ is the phase difference between the two superconducting electrodes, V is the voltage drop across the junction and Φ_o is the flux quantum given by $\Phi_o = h/2e$. The CPR demonstrates that the phase difference between the two superconducting electrodes with an insulating barrier induces a superconducting current which disappears when the phase difference between the two superconducting electrodes disappears. In 2008 Buzdin [1] showed that for some barrier materials (for e.g. ferromagnets) with surface broken inversion symmetry (BIS), (i.e. with a Rashba type (SOC)), and a magnetic field $\vec{h}$ which maybe intrinsic or externally applied, a phase shift φ_o is introduced in the CPR thus it takes the form

$$I_s = I_c \sin(\varphi + \varphi_o), \tag{2}$$

where the phase shift now induces a supercurrent even at zero phase difference between the two superconducting electrodes. This is the so called anomalous φ_o Josephson junction [2].
In this study a ferromagnetic barrier with a Rashba type SOC is used. The dynamics of a magnetic system are known to be described through the Landau-Lifshitz-Gilbert equation while that of a Josephson junction is through the Josephson equations Eq.(1). In a Josephson junction with a ferromagnetic barrier, both systems of equations are coupled together and in this study are solved numerically.
For our junction we use the resistively and capacitively shunted junction (RCSJ) model which we shall briefly outline below. We then review some basics starting with the the Buzdin model then the LLG equation and finally we introduce the system of coupled equations to be solved.

1.1 The RCSJ model

An equivalent circuit [3] of a DC current biased Josephson junction in the framework of the RCSJ model is given in Fig.(1)

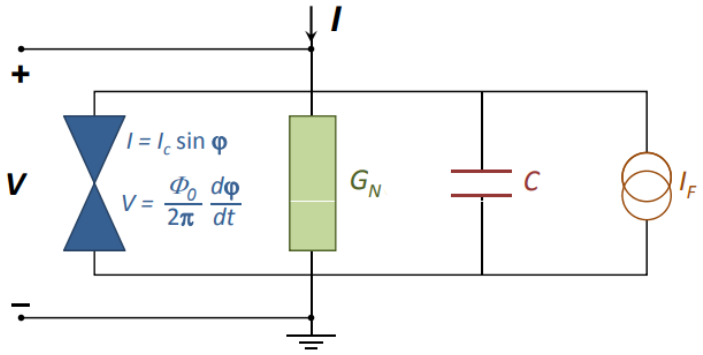

Figure 1: The equivalent circuit for a Josephson junction in the RCSJ approximation model [3].

When the biasing current I does not exceed I_c, this state is referred to as the superconducting state or the zero voltage state where all the current flows as supercurrent and no voltage drop is developed across the junction. If the current exceeds such critical current, the excess flows through a resistive channel, the so called normal current channel creating a potential difference V and a time evolving phase difference. If the potential difference evolves in time as well, the excess current can also flow as a displacement current through a capacitive channel. This state is the so called voltage state. In this case the total current is of course fixed by the fixed biasing current,

$$I = I_s + I_N + I_D + I_F \tag{3}$$

where I_F is a fluctuating noise current that we shall ignore in our treatment of a single junction. I_D is the displacement current given by $I_D = C\frac{dV}{dt}$, I_N is the quasiparticle current given by $G_N(V)V$, where $G_N(V)$ is the normal conductance which we will take as a constant taking the resistively and capacitively shunted junction (RCSJ) Model approximation, $G_N(V) = G_N = \frac{1}{R}$, and I_s is the Josephson supercurrent $I_s = I_c \sin\phi$.
This combined with the Josephson voltage-phase relation Eq.(1) gives

$$\left(\frac{\hbar}{2e}\right) C\frac{d^2\phi}{dt^2} + \left(\frac{\hbar}{2e}\right)\frac{1}{R}\frac{d\phi}{dt} + I_c[\sin\phi - \frac{I}{I_c}] = 0 \tag{4}$$

Normalizing time with respect to the inverse of the characteristic frequency $\tau = t\omega_c$, where $\omega_c = 2eRI_c/\hbar$ and currents with respect to I_c we get the dimensionless form of the latter equation

$$\frac{dv}{d\tau} = \frac{1}{\beta_c}[i - v - \sin\varphi] \tag{5}$$

where the dimensionless voltage-phase relation takes the form

$$\frac{d\varphi}{d\tau} = v, \tag{6}$$

$v = V/I_cR$, $i = I/I_c$ and the Stewart-McCumber parameter given by $\beta_c = 2eI_cCR^2/\hbar$.
We call junctions with ($\beta_c \ll 1$), or equivalently small capacitance and/or resistance, overdamped junctions. While for junctions with ($\beta_c \gg 1$) or equivalently large capacitance and/or resistance, underdamped junctions.
Below the CVC curves for the underdamped and overdamped junctions are shown where β is the dissipation parameter given by $\beta = 1/\sqrt{\beta_c}$.

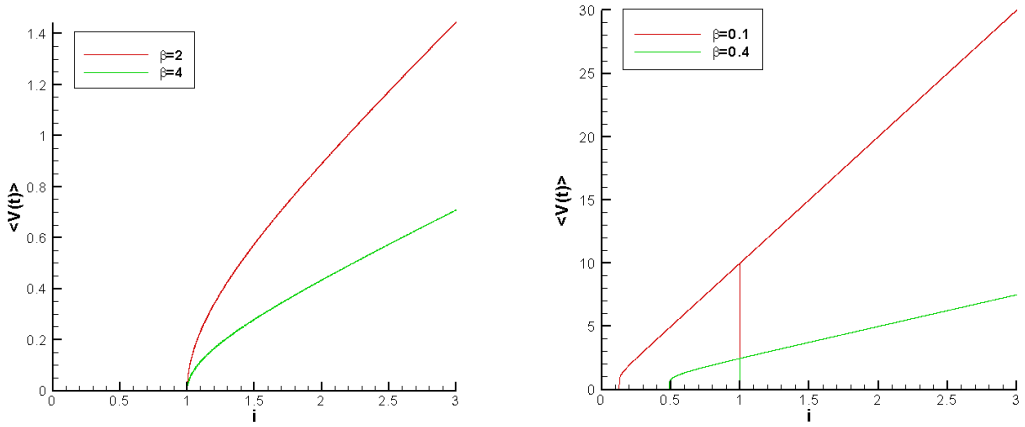

(a) (b)

Figure 2: (b): CVC for an overdamped junction with dissipation parameters $\beta = 2$ and $\beta = 4.$, (c): CVC for an underdamped junction with dissipation parameters $\beta = 0.1$ and $\beta = 0.4$.

1.2 The Buzdin model for an anomalous Josephson junction

The phase shift φ_o in Eq.(2) was derived starting from the Ginzburg-Landau phenomenological model. The free energy density was modified to include the contributions of a Rashba type SOC, which occurs for certain types of materials with surface broken inversion symmetry (BIS) [1], and a magnetic field $\vec{h}$ which may be intrinsic to the system (i.e. an exchange interaction field) or externally applied. Minimizing the Ginzburg-Landau free energy density the CPR for such materials with BIS was derived to include a phase shift φ_o

$$\varphi_o \propto \vec{n}.(\vec{M} \times \vec{\nabla}\psi) \tag{7}$$

where $\vec{n}$ is the direction of the Rashba SOC and $\vec{\nabla}\psi$ is the gradient of the order parameter whose direction is that of the supercurrent flow.

The geometry of the junction in our study is shown in figure(3)

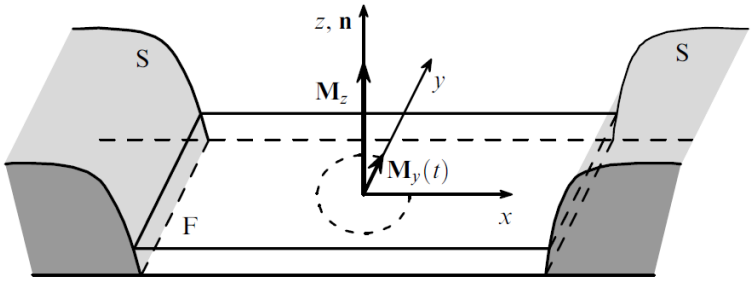

Figure 3: Geometry of the SFS Josephson junction studied in our system [4].

$\vec{n}$ is directed along the z-axis, so is the easy axis of the ferromagnet and $\vec{\nabla}\psi$ is along the x-axis. Thus the only non-vanishing component of $\vec{M}$ contributing to φ_o according to Eq.(7) is M_y and φ_o takes the form $\varphi_o = rm_y$ where r is the SOC parameter and m_y is the y-component magnetization normalized to the M_o, thus finally according to our geometry the CPR takes the form

$$I = I_c \sin(\varphi - rm_y). \tag{8}$$

Below we introduce some basics concerning the Landau-Lifshitz-Gilbert equation for describing the dynamics of the magnetization.

1.3 The Landau-Lifshitz-Gilbert equation

Larmor precession

Let us first discuss the effect of an external magnetic field $\vec{B}$ on a particle with associated magnetic moment $\vec{\mu}$. The potential energy for such an interaction is given by the Zeeman energy

$$W = -\vec{\mu}.\vec{B}, \quad \vec{B} = \mu_o \vec{H} \tag{9}$$

where μ_o is the permeability of free space and $\vec{H}$ is the magnetic field strength. The force exerted on a particle with magnetic moment $\vec{\mu}$ can thus be written as

$$\vec{F} = \vec{\nabla}(\vec{\mu}.\vec{B}) \tag{10}$$

Consequently the torque exerted is given by

$$\vec{\Gamma} = \vec{\mu} \times \vec{B}. \tag{11}$$

From the momentum theorem we know that

$$\frac{d\vec{L}}{dt} = \vec{\Gamma}, \tag{12}$$

where $\vec{L}$ is the angular momentum. Since the angular momentum and the magnetic moment are proportional through the gyromagnetic ratio γ given by $\gamma = |g|\mu_B/\hbar$ where g is the Lande g-factor and μ_B is the Bohr magneton,

$$\vec{\mu} = -\gamma \vec{L}, \tag{13}$$

equation(12) takes the form

$$\frac{d\vec{\mu}}{dt} = -\gamma_o \, \vec{\mu} \times \vec{H} \tag{14}$$

where $\gamma_o = \mu_o \, \gamma$. Thus the vector $\vec{\mu}$ undergoes a precession around the axis of the applied field as shown in figure (4(a))

It is constructive to use the magnetization $\vec{M}$ of a material, which is defined as the magnetic moment per unit volume, instead of just dealing with magnetic moments associated with single particles. It can easily be seen that $\vec{M}$ follows Eq.(14) so that we have

$$\frac{d\vec{M}}{dt} = -\gamma_o \, \vec{M} \times \vec{H} \tag{15}$$

Landau-Lifshitz-Gilbert equation

The landau-Lifshitz equation takes the same form as Eq.(15) but with an $\vec{H}_{eff}$ term containing various contributions including magnetic anisotropy, exchange interaction, external field components etc..instead of only just an external applied field.

$$\frac{d\vec{M}}{dt} = -\gamma_o \, \vec{M} \times \vec{H}_{eff} \tag{16}$$

This was the form derived by Landau and Lifshitz in 1935. The Gilbert damping term was added phenomenologically in 2004 in order to account for the experimental results for ferromagnetic materials where beyond critical values the magnetization aligns parallel to the applied field.

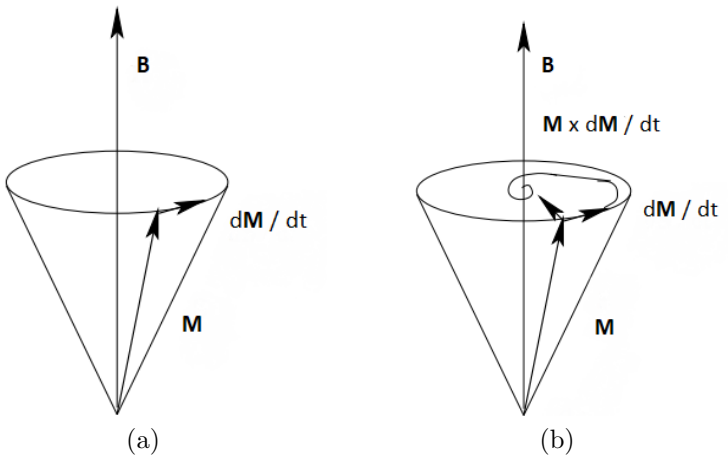

Figure 4: (a): Magnetization precession without damping, (b): Magnetization precession with the Gilbert damping included [5].

The Landau-Lifshitz-Gilbert equation with the Gilbert damping term takes the form

$$\frac{d\vec{M}}{dt} = -\gamma_o \vec{M} \times \vec{H}_{eff} + \frac{\alpha}{M_o}\vec{M} \times \frac{d\vec{M}}{dt} \tag{17}$$

where α is the damping parameter and $\vec{M} = M_o \vec{m}$, M_o being the modulus of the magnetization vector and $\vec{m}$ a unit magnetization vector. The precession including the damping term is now dissipative and can be illustrated by figure (4(b)).

Eliminating the time derivative from the right hand side of the equation

It is convenient to reformulate Eq.(17) so that the time derivative can be separated in one side. Taking the cross product of $\vec{M}$ with Eq.(17) we get

$$\vec{M} \times \frac{d\vec{M}}{dt} = -\gamma_o \vec{M} \times (\vec{M} \times \vec{H}_{eff}) + \frac{\alpha}{M_o}\vec{M} \times (\vec{M} \times \frac{d\vec{M}}{dt}) \tag{18}$$

using basic vector identities the cross product for the second term on the right hand side can be written as

$$\vec{M} \times (\vec{M} \times \frac{d\vec{M}}{dt}) = (\vec{M}.\frac{d\vec{M}}{dt})\,\vec{m} - (\vec{M}.\vec{M})\frac{d\vec{M}}{dt} \tag{19}$$

since $\vec{M}.\vec{M} = M_o^2$ and $\vec{M}.\frac{d\vec{M}}{dt} = 0$ (this can be easily seen by taking the dot product of $\vec{M}$ with Eq.(17) since the right hand side vanishes), thus Eq.(18) takes the form

$$\vec{M} \times \frac{d\vec{M}}{dt} = -\gamma_o \vec{M} \times (\vec{M} \times \vec{H}_{eff}) - \alpha M_o \frac{d\vec{M}}{dt} \tag{20}$$

substituting with this in the last term of Eq.(17) we finally get

$$\frac{d\vec{M}}{dt} = -\frac{\gamma_o}{1+\alpha^2}\vec{M}\times\vec{H}_{eff} - \frac{\gamma_o\alpha}{M_o(1+\alpha^2)}\vec{M}\times(\vec{M}\times\vec{H}_{eff}) \tag{21}$$

This is the form that we are going to be using in our simulations.

2 Model

For an RCSJ model the dimensionless Josephson equations for an SFS junction with currents normalized to I_c, time normalized to the inverse of the characteristic frequency $\omega_c = 2eRI_c/\hbar$ and M_y normalized to M_o take the form

$$\begin{aligned} \frac{dv}{d\tau} &= \frac{1}{\beta_c}[i - v - \sin(\varphi - rm_y) + r\frac{dm_y}{d\tau}], \\ \frac{d\varphi}{d\tau} &= v. \end{aligned} \tag{22}$$

where β_c is the Stewart-McCumber parameter given by $\beta_c = 2eI_cCR^2/\hbar$.
In order to solve this numerically we need to find $\dot{m}_y$ and since the dynamics of the magnetization are solved through the LLG, the two systems, magnetic and Josephson, are coupled through m_y.

2.1 System of equations without electromagnetic radiation

In order to solve the coupled system of equations we need to know what the effective field $\vec{H}_{eff}$ of our system looks like. Generally the effective field can be calculated through taking the first order variation of the free energy of the system [6]

$$\vec{H}_{eff} = -\frac{1}{\mu_o}\frac{\delta F}{\delta\vec{M}} \tag{23}$$

In our system it takes the form [1]

$$\vec{H}_{eff} = \frac{K}{\mu_o M_o}[Gr\sin(\varphi - rm_y)\hat{e}_y + m_z\hat{e}_z] \tag{24}$$

where K is the anisotropic constant and G is the ratio E_J/KV, V being the volume of the ferromagnetic layer.
The first term in Eq.(24) stems from the energy contribution of the Josephson system and the second stemming from the energy contribution of the magnetic anisotropy of the ferromagnet. Substituting with the effective field Eq.(24) in the LLG Eq.(21) and again normalizing time

with respect to ω_c^{-1} and M_i, $(i = x, y, z)$ with respect to M_o we get the following system of equations

$$\begin{aligned}
\dot{m}_x &= \frac{\omega_F}{1+\alpha^2}\{-m_y m_z + Grm_z \sin(\varphi - rm_y) - \alpha[m_x m_z^2 + Grm_x m_y \sin(\varphi - rm_y)]\} \\
\dot{m}_y &= \frac{\omega_F}{1+\alpha^2}\{m_x m_z - \alpha[m_y m_z^2 - Gr(m_z^2 + m_x^2)\sin(\varphi - rm_y)]\} \\
\dot{m}_z &= \frac{\omega_F}{1+\alpha^2}\{-Grm_x \sin(\varphi - rm_y) - \alpha[Grm_y m_z \sin(\varphi - rm_y) - m_z(m_x^2 + m_y^2)]\}
\end{aligned} \tag{25}$$

where ω_F is the ratio between the ferromagnetic resonance (FMR) frequency $\Omega_F = \gamma K/M_o$ and the characteristic frequency ω_c, i.e. $\omega_F = \Omega_F/\omega_c$.

2.2 System of equations with the magnetic component of EMR

If we include a magnetic component $H_R \sin(\omega_R \tau)$ of an EMR with amplitude H_R and frequency ω_R to be directed along the easy-axis, z-axis, of our system the effective field is modified to be

$$\vec{H}_{eff} = \frac{K}{\mu_o M_o}[Gr \sin(\varphi - rm_y)\hat{e}_y + m_z \hat{e}_z] + H_R \sin(\omega_R \tau)\hat{e}_z \tag{26}$$

The former set of equations is thus modified to be

$$\begin{aligned}
\dot{m}_x &= \frac{\omega_F}{1+\alpha^2}\{-m_y m_z + Grm_z \sin(\varphi - rm_y) - \alpha[m_x m_z^2 + Grm_x m_y \sin(\varphi - rm_y)]\} \\
&\quad - \frac{h_R \sin(\omega_R \tau)}{1+\alpha^2}[\alpha m_x m_z + m_y] \\
\dot{m}_y &= \frac{\omega_F}{1+\alpha^2}\{m_x m_z - \alpha[m_y m_z^2 - Gr(m_z^2 + m_x^2)\sin(\varphi - rm_y)]\} \\
&\quad - \frac{h_R \sin(\omega_R \tau)}{1+\alpha^2}[\alpha m_y m_z - m_x] \\
\dot{m}_z &= \frac{\omega_F}{1+\alpha^2}\{-Grm_x \sin(\varphi - rm_y) - \alpha[Grm_y m_z \sin(\varphi - rm_y) - m_z(m_x^2 + m_y^2)]\} \\
&\quad - \frac{h_R \sin(\omega_R \tau)}{1+\alpha^2}[\alpha(m_x^2 + m_y^2)]
\end{aligned} \tag{27}$$

where $h_R = \gamma_o H_R/\omega_c$.

3 Results

We now demonstrate simulation results focusing separately on the effect of the electric component of the EMR, the magnetic component and then both components. We study in the latter case the effect of the SOC parameter r, the amplitude of the electric component and the amplitude

of the magnetic component on the maximum y-component magnetization. In our simulations we use $\omega_F = 0.5$, $\omega_R = 0.485$ and an underdamped junction with $\beta_c = 25$.

3.1 CVC and magnetization for a φ_o junction without external radiation

We demonstrate the effect of the SOC parameter on the CVC and the magnetization without any external radiation [7]. The effect of increasing the SOC on the CVC can be seen in Fig.(5). A nonlinear region appears around normalized voltage value equal to ω_F. The (SOC) parameter r is increased from 0.1 to 1 in steps of 0.1. An interesting feature appears for $r > 0.4$ where a negative differential resistance (NDR) starts developing, it should also be noted that the nonlinearity starts shifting downwards on increasing r. Corresponding to such nonlinearities in the magnetization curves is a FMR phenomena, where the resonance peak is increased on increasing r and shifted towards the right as illustrated in the figure below.

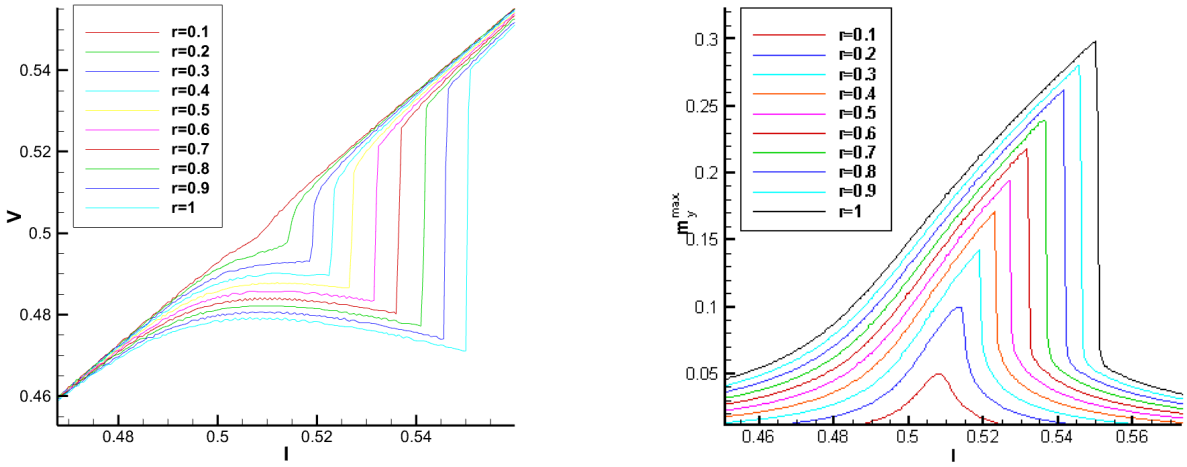

(a) (b)

Figure 5: (a): CVC curves showing NDR on increasing the SOC parameter r, (b): corresponding y-component magnetization showing a FMR.

3.2 The effect of the electric component only

The effect of adding an electric component on our system of equations modifies only Eq.(22) to include the term $A\sin(\omega_R\tau)$, where A is the amplitude of the electric component normalized to

the critical current I_c so that Eq.(22) takes the form

$$\frac{dv}{d\tau} = \frac{1}{\beta_c}[i + A\sin(\omega_R\tau) - v - \sin(\varphi - rm_y) + r\frac{dm_y}{d\tau}], \tag{28}$$

The system of coupled equations (28) and (25) are solved together numerically using a fourth order Runge-Kutta method. An interesting result is demonstrated below [7], when the normalized voltage equals the radiation frequency i.e. when the Josephson frequency $\omega_J = \omega_R$, a shapiro step appears, for some values of SOC parameter r to be separated by a bump representing the nonlinearity. Fig.(6) highlights this effect (red curve) for $r = 0.56$ and $A = 0.1$. This is reflected on the magnetization curve (green curve) as two locking regions, represented by the steps of the same widths, having the same frequency as ω_R but the amplitude of the higher step is higher.

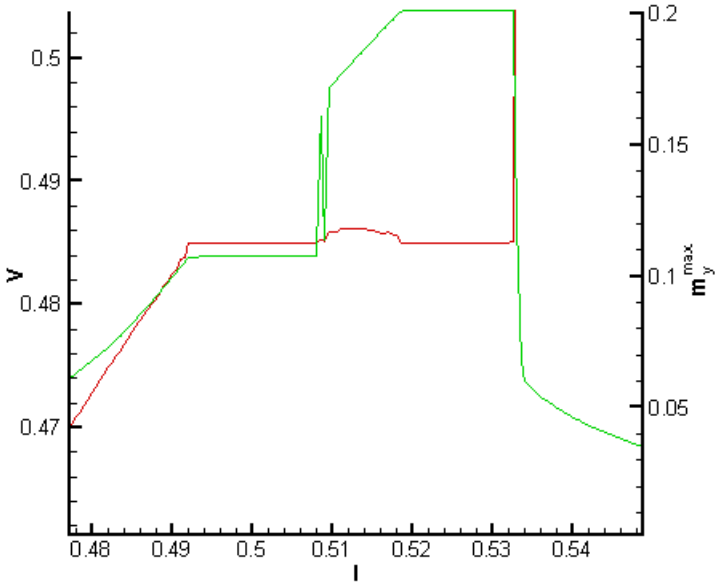

Figure 6: Effect of the electric component on the CVC (red curve) and y-component magnetization (green curve) for $A = 0.1$, $r = 0.56$.

3.3 The effect of the magnetic component only

On including the magnetic component only, the system of equations (22) and (27) is solved numerically. Fig.(7) below demonstrates two main features, a resonance splitting, and a locking phenomenon as the latter case. It should be noted however that the reflection of the step in the CVC on the magnetization curve does not correspond to a locking region of constant amplitude as before, but is reflected as "bubble" representing changing amplitude [8], but the system is still locked with the same frequency ω_R. It should also be noted that the resonance involved

here is a different type of resonance from that involved in the case without radiation or with the electric component only [8]. The former is due to direct interaction of the magnetization in the system with the external magnetic component while the latter doesn't depend on the external radiation but the FMR of the system $\Omega_F = \gamma K/M_o$ or when normalized to ω_c written as $\omega_F = \Omega_F/\omega_c$. Fig.(7) below demonstrates the effect for $r = 0.56$ and $h_R = 1.7$.

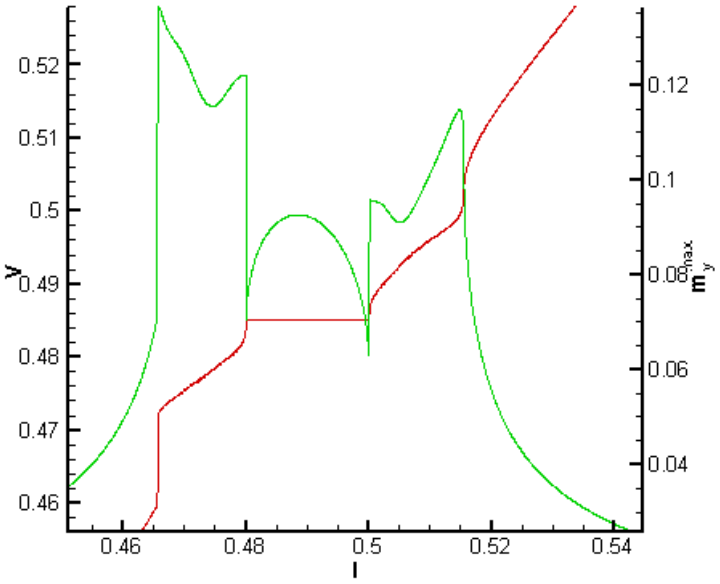

Figure 7: Effect of the magnetic component on the CVC (red curve) and y-component magnetization (green curve) for $h_R = 1.7$, $r = 0.56$.

3.4 The effect of both the electric and magnetic components

Including both the EMR components we solve the system of equations (28) and (27) numerically. in this case, for the same parameters, we observe the interesting phenomena where a second smaller "bubble" appears to the left hand side shown in Fig.(8) . The nature of this bubble is still unknown but in a following subsection we demonstrate, for certain values of parameters, the ability to control its width.

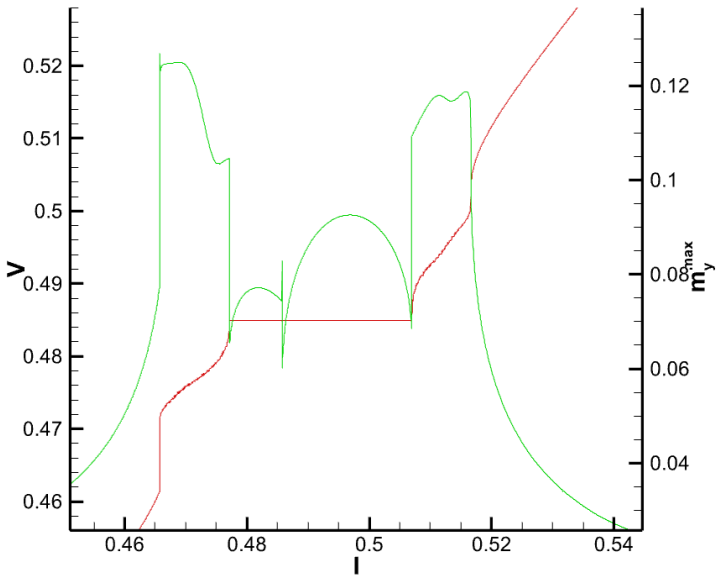

Figure 8: Effect of both EMR components on the CVC (red curve) and y-component magnetization (green curve) for $A = 0.1$, $h_R = 1.7$ and $r = 0.56$.

3.4.1 The effect of changing the amplitude of the magnetic component

The evolution of the magnetization curve for $r = 0.4$ on increasing h_R from 0 to 2.6 can be divided into regions showing similar behavior as will be discussed. The overall trend features a resonance splitting, a locking phenomenon and magnetization oscillations due to the application of the external magnetic field.

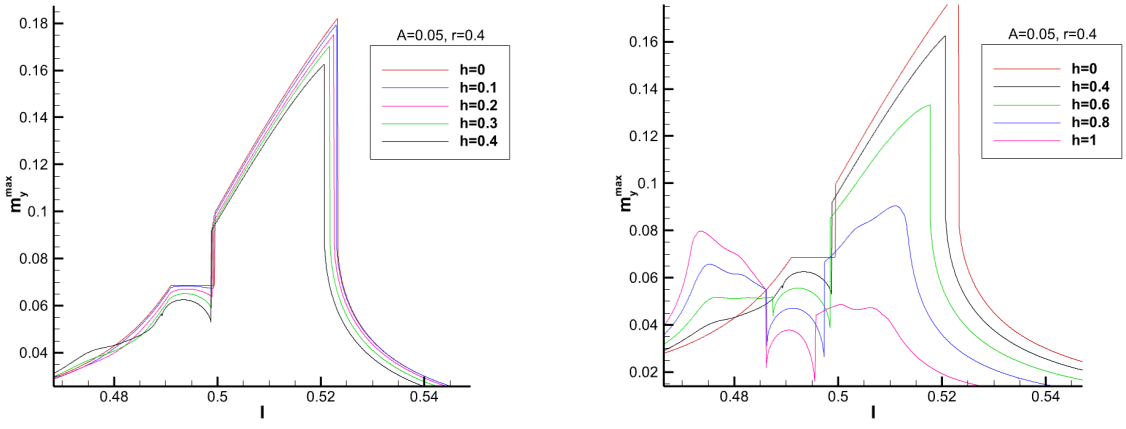

(a) (b)

Figure 9: The figures demonstrate the effect of increasing h_R, labeled h in the figures, where $A = 0.05$.

Starting from $h_R = 0.1$ we see in Fig.(9(a)) the magnetization curve shape slightly deviate from that of $h_R = 0$, the step is slightly curved, however, maintaining the locking phenomenon, the resonance peak is slightly shifted downwards and to the left. $h_R = 0.2$ and 0.3 show similar behavior with the peak falling nonlinearly with h_R increase. On increasing h_R to 0.4, shown in Fig.(9(b)), a slight rise with a small spike can be seen on the left hand side to the bubble. A resonance peak shall rise on increasing h_R while the right hand side peak continues to fall. It should be noted that the width of the bubble increases as it is shifted downwards. This continues till a flipping point is reached at $h_R = 0.9$ where now the left hand side peak becomes higher than the right, the width then decreases on increasing h_R till reaching $h_R = 1.1$.
From $h_R = 1.1$, Fig.(10(a)) an interesting feature can be seen, a second bubble begins to form. On reaching 1.4, Fig.(10(b)) the two bubbles become more pronounced, the whole curve shifts upwards and the two bubbles widen pushing the two resonance peaks outwards. This continues up until 1.9 where again the right hand side peak is flipped higher than the left. The two bubbles width decreases. Similar results were also obtained for $r = 0.7$.

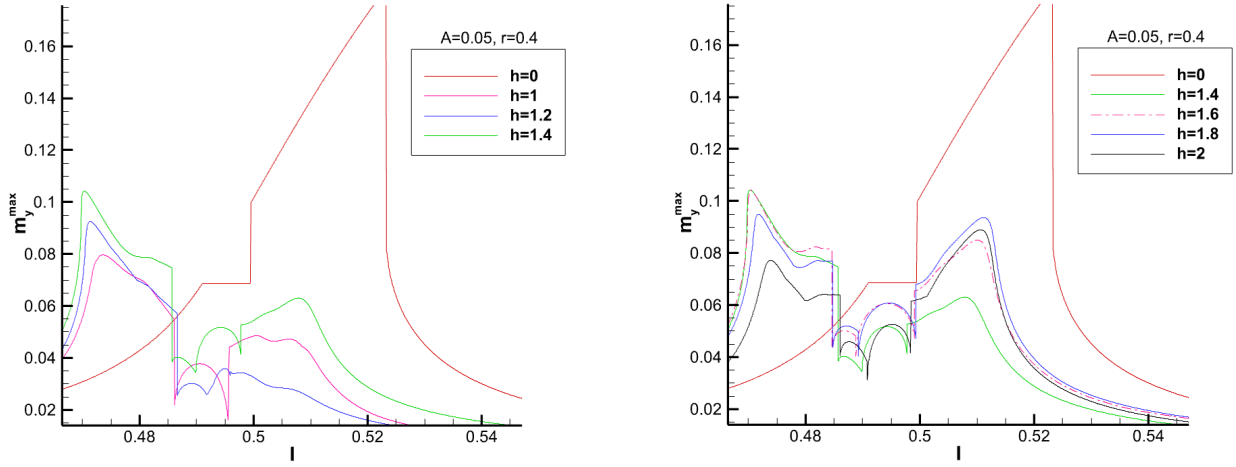

(a) (b)

Figure 10: The figures demonstrate the effect of increasing h_R, labeled h in the figures, where $A = 0.05$.

3.4.2 The effect of changing the amplitude of the electric component

We demonstrate the effect for two values of SOC, $r = 0.4$ whose level is around $v = 0.485$ and for $r = 0.7$ whose level is below it. The CVC and magnetization curves for both cases are presented in Fig.(11)below with parameters $A = 0.05$ and $h_R = 1.7$.

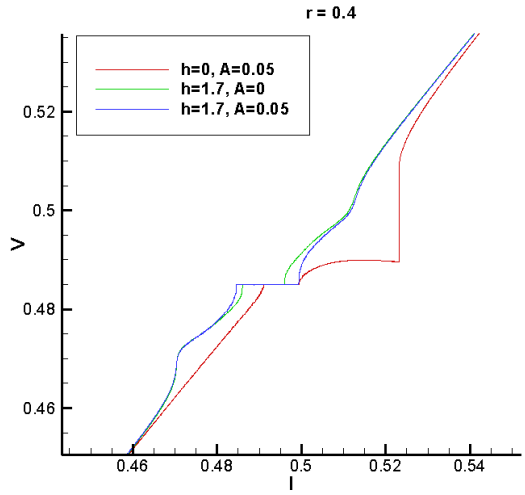

(a)

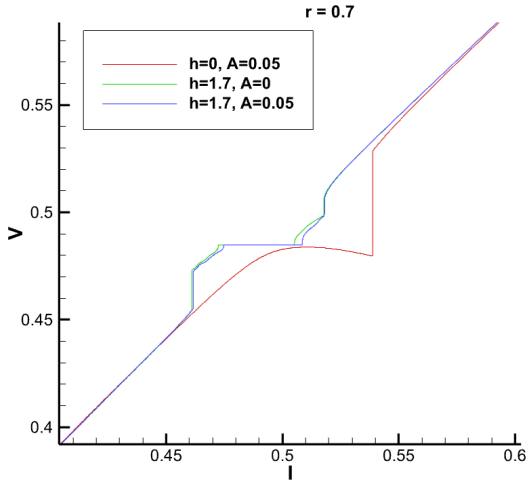

(b)

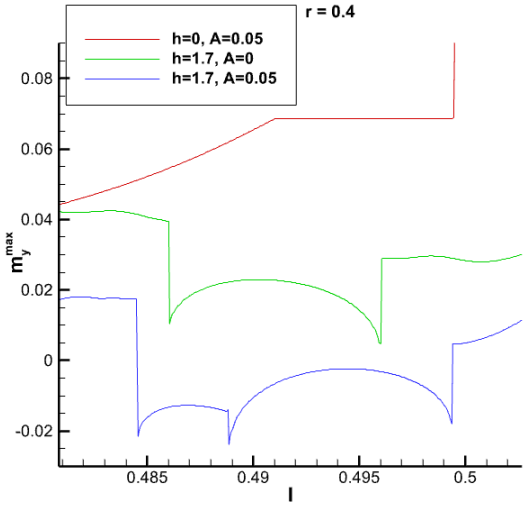

(c)

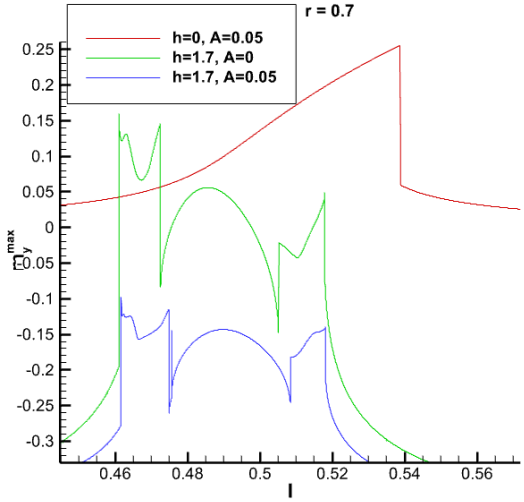

(d)

Figure 11: (a), (b): CVC curves for the three cases, for $r = 0.4$ on the left hand side and $r = 0.7$ on the right hand side, (c), (d): show the corresponding magnetization curves, note that there are three scales, not shown, one for each, the scales have been adjusted to emphasize the shape of each one separately.

We start with amplitude $A = 0$ and increment it in units of 0.01 till $A = 0.1$. The effect for $r = 0.4$ is demonstrated below in Fig.(12).

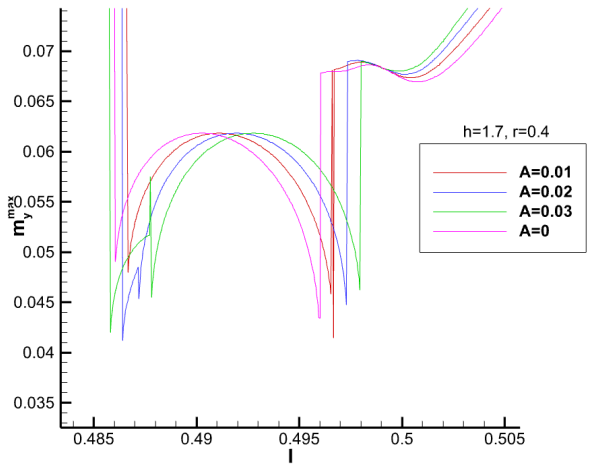

(a)

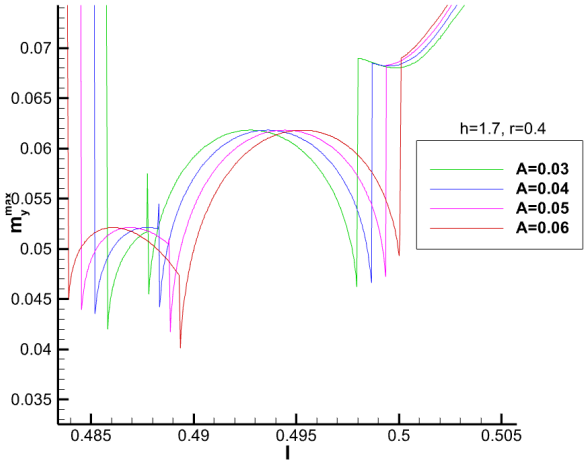

(b)

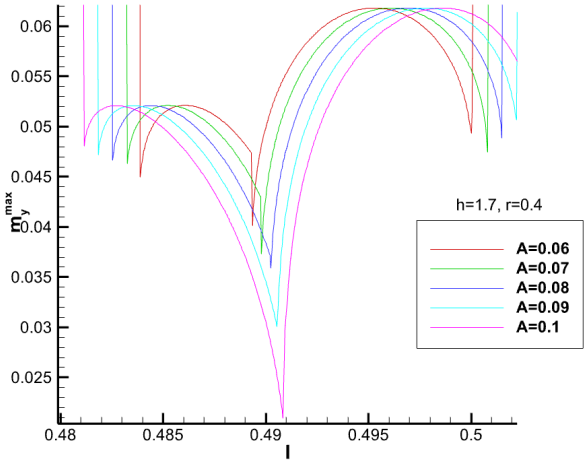

(c)

Figure 12: The figures demonstrate the evolution and width change of the smaller bubble for $r = 0.4$.

It can be seen that as A increases the smaller bubble begins to form and its width increases while the larger one's width remain nearly constant. The data for the widths vs A is presented in Fig.(13).

A	W_L	W_s
0	0.00995	0
0.01	0.00999	0
0.02	0.01011	0.00079
0.03	0.01015	0.00203
0.04	0.01028	0.00317
0.05	0.01054	0.00425
0.06	0.01073	0.00544
0.07	0.011	0.00658
0.08	0.01123	0.00769
0.09	0.01169	0.0087
0.1	0.01242	0.00965

(a)

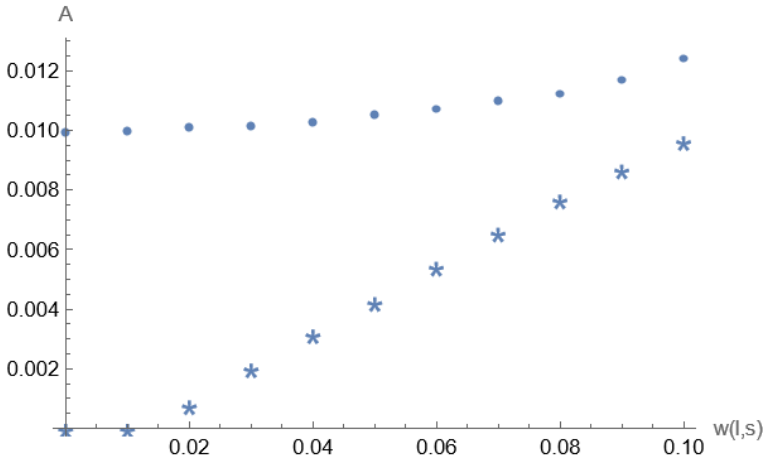

(b)

Figure 13: Width change of both bubbles vs the amplitude A.

Figure (13) illustrates the fact noticed in figures (12), it can be seen that the change in width of the larger bubble W_L isn't that great with respect to the smaller one whose width W_s increases steadily with A.

A similar result is also demonstrated for the $r = 0.7$ case.

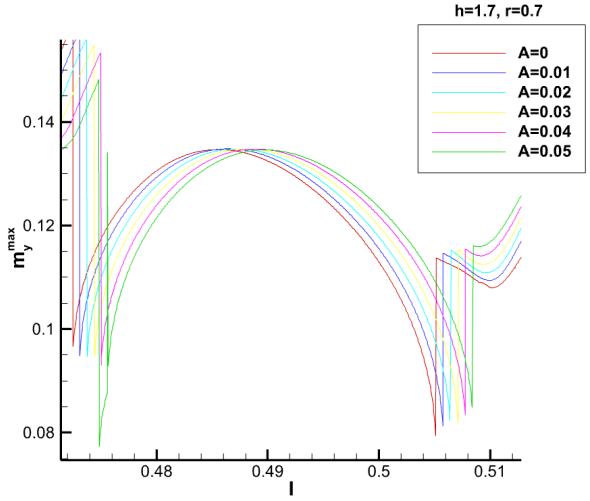

(a)

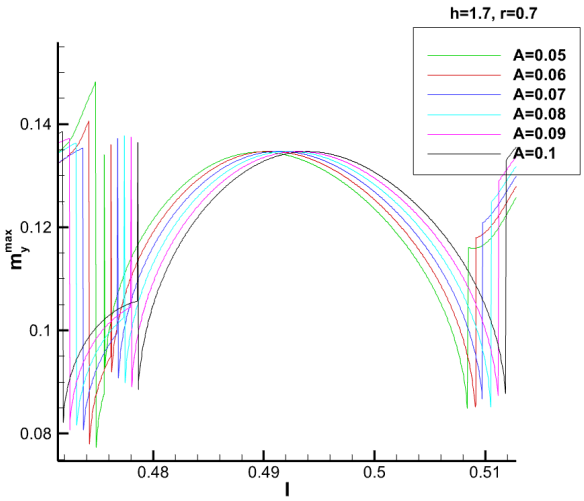

(b)

Figure 14: The figures demonstrate the evolution and width change of the smaller bubble for $r = 0.7$.

A	w_L	w_s
0	0.03264	0
0.01	0.0327	0
0.02	0.03264	0
0.03	0.03269	0
0.04	0.0327	0
0.05	0.03288	0.0007
0.06	0.03289	0.0019
0.07	0.03288	0.00306
0.08	0.03307	0.00426
0.09	0.03319	0.00552
0.1	0.03319	0.00671

(a)

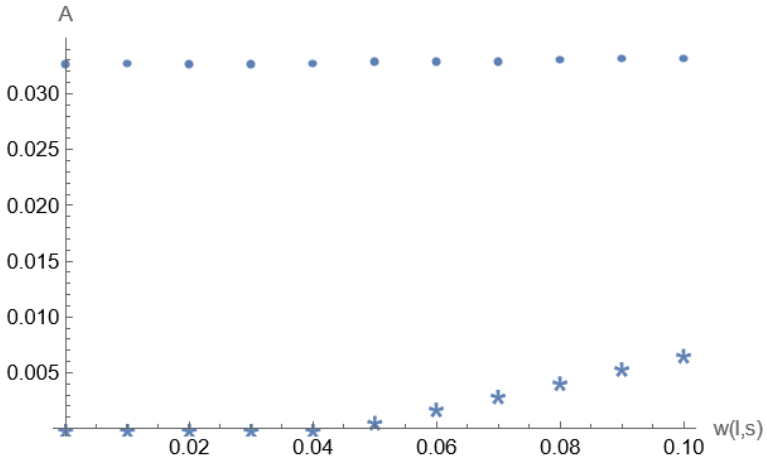

(b)

Figure 15: The figures demonstrate the evolution and width change of the smaller bubble for $r = 0.7$.

4 Conclusion

In this study we demonstrated some interesting features for the anomalous φ_o SFS Josephson junction. Ferromagnetic resonance and negative differential resistance phenomena have been shown for a φ_o without any external radiation. Application of the electric component introduced a locking phenomena leading to the appearance of constant amplitude magnetization steps with the same width as the Shapiro steps appearing in the CVC. The effect of the magnetic field component has also been studied where instead of a step appearing in the magnetization curve, a bubble-like feature appears. The width of the corresponding CVC step in this case is dependent on r. Intriguing results have been obtained by including both components together. A second bubble whose nature is yet to be known appears, and for some parameters we demonstrated the ability to control its width. We also demonstrated the effect of the amplitude of the magnetic component on the behavior of the magnetization curves. The effect of both the electric and magnetic components shows many interesting features which are yet to be explained.

5 Acknowledgements

Firstly I would like to thank JINR for providing such opportunity for young researchers to be immersed in this great research environment. I would also like to express my utmost gratitude to my supervisor, Dr. Majed Nashaat AbdelGhani for his patience, careful guidance, eagerness to share his knowledge, fruitful discussions and introducing me to new concepts and tools

throughout this period. I would also like to thank Prof. Yu. M. Shukrinov for giving me the opportunity to be involved in an ongoing research topic during this training period and for his guidance as well and special thanks to Prof. Yu. M. Shukrinov research group for providing me the code of calculations. And lastly I would like to thank my colleagues for all their help, encouragement and support.

References

[1] Buzdin A 2008 *Physical Review Letters* **101**(10) 107005 ISSN 0031-9007

[2] Shukrinov Y M 2022 *Physics-Uspekhi* **65**(4) 317–354 ISSN 1063-7869

[3] Gross R, Marx A and Deppe F 2016 *Applied Superconductivity: Josephson Effect and Superconducting Electronics* De Gruyter Textbook (De Gruyter) ISBN 9783110417067

[4] Konschelle F and Buzdin A 2009 *Physical Review Letters* **102**(1) 017001 ISSN 0031-9007

[5] Lakshmanan M 2011 *Philosophical Transactions of the Royal Society A: Mathematical, Physical and Engineering Sciences* **369**(1939) 1280–1300 ISSN 1364-503X

[6] Dieny B, Goldfarb R and Lee K J 2017 *Introduction to Magnetic Random-Access Memory* ISBN 9781119079415

[7] Abdelmoneim S A, Shukrinov Y M, Kulikov K V, ElSamman H and Nashaat M 2022 *Physical Review B* **106**(1) 014505 ISSN 2469-9950

[8] Shukrinov Y M, Kovalenko E, Tekic J, Kulikov K and Nashaat M 2023